RESEARCH ARTICLE

PLANT SCIENCE

Enhancing rice panicle branching and grain yield through tissue-specific brassinosteroid inhibition

Xiaoxing Zhang[1]†, Wenjing Meng[1]†, Dapu Liu[1]†, Dezhuo Pan[2]†, Yanzhao Yang[1], Zhuo Chen[3], Xiaoding Ma[1], Wenchao Yin[1], Mei Niu[1], Nana Dong[1], Jihong Liu[1], Weifeng Shen[2], Yuqin Liu[2], Zefu Lu[1], Chengcai Chu[3], Qian Qian[1]*, Mingfu Zhao[2]*, Hongning Tong[1]*

C........d......7......7.d...7.d...7...7.......7........7.....
7.d.....B.7......d (BR)...................7...7........
.....7..B.d.....................7...7.......77..7...........BR
.77.....7...... BRASSINOSTEROID-DEFICIENT DWARF3 (BRD3) .7....7.......7........
...7....7.......7...BR......... GSK3/SHAGGY-LIKE KINASE2
.......7....7..d...7....O..MAD...1.7.......7.7...........7..... TERMINAL FLOWER1-....
.....RICE CENTRORADIALIS2........7..7........BRD3...........7...7........O..
..d.......7........7.................7....7.d......7.....7....d..O..
7...7.7....7...7.d...7......7....................7.d.......

Here, we report our successful cloning of the causal gene for CL by large-scale screening of CL suppressor mutants. We show that CL is associated with complex chromosome structural variations, which activate the expression of the BR catabolic gene *BRASSINOSTEROID-DEFICIENT DWARF3* (*BRD3*) in the secondary branch meristems and pedicels. Notably, the spatial-specific activation of *BRD3* promotes grain number while avoiding the commonly seen negative effects of BR deficiency on grain size and grain quality. Moreover, we establish a complete BR pathway for mediating BR regulation of panicle branching. Furthermore, we demonstrate that introduction of *CL* into various backgrounds, either containing *Gn1a* gene or not, can substantially improve rice yield.

Results

CL confers enhanced panicle branching and grain yield

CL1 represents a typical CL variety characterized by clustered growth, primarily consisting of three grains. To facilitate comparisons, we generated a non-CL variety (NCL1) by using CL1 as the recurrent parent. Apart from the distinct panicle morphology, no other notable differences were observed between NCL1 and CL1 (Fig. 1, A and B). The clustered growth in CL1 predominantly occurred at the terminus of the secondary branch, where a pair of closely fused spikelets formed, with a third spikelet attached nearby (Fig. 1, C and D). Additionally, the tertiary branch was frequently observed in CL1 but not in NCL1 plants (Fig. 1E). Moreover, pedicels attached to the spikelets in CL1 were shorter than those of NCL1 (Fig. 1F).

CL1 showed a 28.2% increase in grain number per panicle compared to NCL1 (Fig. 1G), which was attributed to a greater number of secondary panicle branches (35.2% increase) and associated spikelets, but not the primary branches (Fig. 1, H to J). No significant differences were detected between NCL1 and CL1 for other traits such as panicle length, panicle number, heading date, and 1000-grain weight (Fig. 1, K to M, and fig. S1). The specific enhancement of grain number in CL1 resulted in a 20.1% increase in grain yield per plant in Beijing (north of China, 2021), 21.7% increase in Sanya (south of China, 2022), and 12.8% increase in Fuzhou (south of China, 2020) compared to NCL1 (Fig. 1, N and O, and fig. S1). These findings were further confirmed in the field plot tests. Under the field conditions, except for the CL phenotype, no other differences were observed throughout NCL1 and CL1 growth (Fig. 1P). Compared to NCL1, CL1 grain yield per hectare averaged 20.96, 17.99, and 11.27% higher in Beijing, Sanya, and Fuzhou, respectively (Fig. 1Q and fig. S1). Regarding grain quality, no significant differences were detected between NCL1 and CL1 in terms of grain chalkiness, amylose content, gel consistency,

ice (*Oryza sativa*) is an essential staple crop, feeding more than half of the world's population (*1*). With global population growth and diminishing arable land, it is crucial to enhance rice grain yield per unit area to ensure global food security. During the development of the rice panicle, the inflorescence meristem produces multiple primary and secondary branches. Panicle branching determines grain number, one of the determinants of grain yield. Therefore, one promising approach to increase grain yield is by enhancing panicle branching. The identification of genes controlling panicle branching, such as *Grain number1a* (*Gn1a*) and *DENSE PANICLE 1* (*DEP1*), has exemplified the success of this approach (*2*, *3*). However, after extensive breeding efforts using these genes, rice yield has reached a plateau, primarily attributed to the intricate trade-offs among various traits that prove resistant to conventional breeding interventions. Tackling this formidable challenge requires an exploration of pioneering genetic reservoirs sourced from a wide array of germplasm resources to facilitate subsequent advancements.

Brassinosteroids (BRs) are a class of steroid phytohormones that play diverse roles in plant growth and development (*4*–*6*). BR responses require BR signaling, in which GSK3/SHAGGY-like kinases, such as BRASSINOSTEROID INSENSITIV2 in the model plant *Arabidopsis*

(*Arabidopsis thaliana*) and GSK3/SHAGGY-LIKE KINASE2 (GSK2) in rice, act as the central inhibitors (*7*, *8*) targeting different substrates to modulate various BR responses (*5*, *9*). In cereal crops such as rice, BRs regulate important agronomic traits such as plant height, leaf angle, and grain size (*5*). Rice mutants with defective BR synthesis or signaling usually show dwarfism, upright leaves, and small grains (*10*–*12*). Despite the promising results achieved in major crops such as rice, maize (*Zea mays*), and wheat (*Triticum aestivum*) using BR-related gene resources for yield improvement (*13*–*15*), the small-grain phenotypes limit the utility of BR mutants for enhancing grain yield. In addition, it remains largely unclear how BRs regulate panicle branching and grain number. Together with additional potential influences such as stress tolerance, the pleiotropic effects of BRs present great challenges for the effective utilization of BR regulatory genes (*5*).

Unlike the common single-grained rice, clustered-spikelet rice (CL), also known as compound-spikelet rice, wheat-spike rice, or SAN-LI-QI (meaning triple-grain-miracle in Chinese), is an unusual rice germplasm possessing an extraordinary trait of multiple (often triple) complete spikelets or grains clustered on the panicles. Since its description early in 1931, the distinctive character of CL has been used to construct a genetic linkage map by worldwide rice geneticists (*16*–*19*). Owing to its potential for improving grain productivity, researchers have made numerous efforts to identify and clone the gene (*CL*) responsible for this trait. Although several studies have successfully mapped the *CL* locus to a specific region on chromosome 6 (*20*–*24*), the gene itself has eluded cloning attempts, for reasons that are unclear.

[1]State Key Laboratory of Crop Gene Resources and Breeding, Institute of Crop Sciences, Chinese Academy of Agricultural Sciences, Beijing 100081, China. [2]Rice Research Institute, Fujian Academy of Agricultural Sciences, Fuzhou 350018, China. [3]Institute of Genetics and Developmental Biology, Chinese Academy of Sciences, Beijing 100101, China.
*C........7.....E.7.........@.77....(H. .); ....@163..(M. .); .7..7.@.77....(Q.Q.)
†These authors contributed equally to this work.

acquire the SM identity. Finally, the SM is transformed into a floral meristem (FM) (25–27). Scanning electron microscopic (SEM) observation identified excrescent SBMs in CL1 at the early stage of panicle development (fig. 1S). In addition, the transition from BM to SM was delayed in CL1 (Fig. 1, S to U). FMs were formed in NCL1 when the young panicle of CL1 was at the SM stage (Fig. 1T), and the FMs were already fully developed in NCL1 when the FMs in the young panicle of CL1 were formed (Fig. 1U). The delay in the transition from BM to SM resulted in prolonged time for generating more SBMs and even the formation of tertiary branches in CL1 (Fig. 1E). Furthermore, an additional SM developed adjacent to the terminal spikelet (Fig. 1U). Pedicel elongation was clear in NCL1 but barely observed in CL1 (Fig. 1V). On the basis of these observations, we concluded that three developmental phenomena drive CL formation: (i) the development of more SBMs, (ii) the initiation of supernumerary SM, and (iii) shortened pedicels.

Cloning the causal gene through screening CL suppressors

To help us track down the genetic basis for CL, we requested three other CL germplasms (CL2, CL3, CL4) from different sources, including one (CL3, IRIS_313-11403) from the 3000 Rice Genomes Project (3K-RG) (28). All three showed the typical CL phenotype, but they exhibited highly variable plant architecture and panicle morphology (fig. S3). We crossed them with each other and found that all F_1 plants derived from the different crosses retained the CL phenotype (fig. S3). By contrast, F_1 plants derived from crosses between CL1 and 9311, an NCL *indica* variety, or between CL1 and Zhonghua11 (ZH11), an NCL *japonica* variety, showed only a weak CL phenotype (WCL), characterized by clustered growth of two grains at the terminus of the panicle branches (figs. S4 and S5). In addition, in the crossed CL1 × ZH11 F_2 population, the segregation ratios (NCL:WCL:CL) were 65:131:45 (fig. S5), close to 1:2:1 ($c^2 = 0.0951664 < 5.99$ at $P = 0.05$). These results suggested that the distinctive phenotype of these CL plants is determined by the same semidominant locus. However, our intense efforts using either map-based cloning or bulked-segregant analysis (BSA) by generating large populations or different crosses could only locate the locus to the ~22.85- to 23.85-Mb (megabase) region on chromosome 6 (fig. S6), like previously reported attempts (21–24). One possibility is that there exist complex chromosome structural variations around the region.

The failure of these routine cloning methods prompted us to design a strategic cloning roadmap by generating large-scale mutagenesis of CL1 for identifying the causal gene (Fig. 2A). From a population of 10,000 independent mutant lines (M_1) using sodium azide as the mutagen, examination of the phenotypes of the M_2 plants (16 for each line) led to the identification of two mutant lines that reverted to a wild-type NCL phenotype, which we designated *cl1-1* and *cl1-2* (Fig. 2B and fig. S7). By comparing the NCL and CL plants pooled from the F_2 population of the *cl1* × CL1 backcrosses, we found that, similar to NCL1, both *cl1-1* and *cl1-2* had significantly decreased grain number compared to CL1, owing to their smaller numbers of secondary branches (Fig. 2, D to F). Both mutants also showed identical plant architecture, panicle number, panicle length, and 1000-grain weight to those of NCL1 and CL1 (figs. S8 and S9 and Fig. 2G). In addition, the grain yield per plant of the two *cl1* mutants decreased by 16.4% to 27.7% compared to CL1 in Sanya (Fig. 2H). Because CL is controlled by a single semidominant

A

NaN₃

CL1

⊗

screen

cl1

B

I

J

K

cl1-1×CL1   cl1-2×CL1

5   17

84   55

1

1

CL1×9311   66   CL1×ZH11
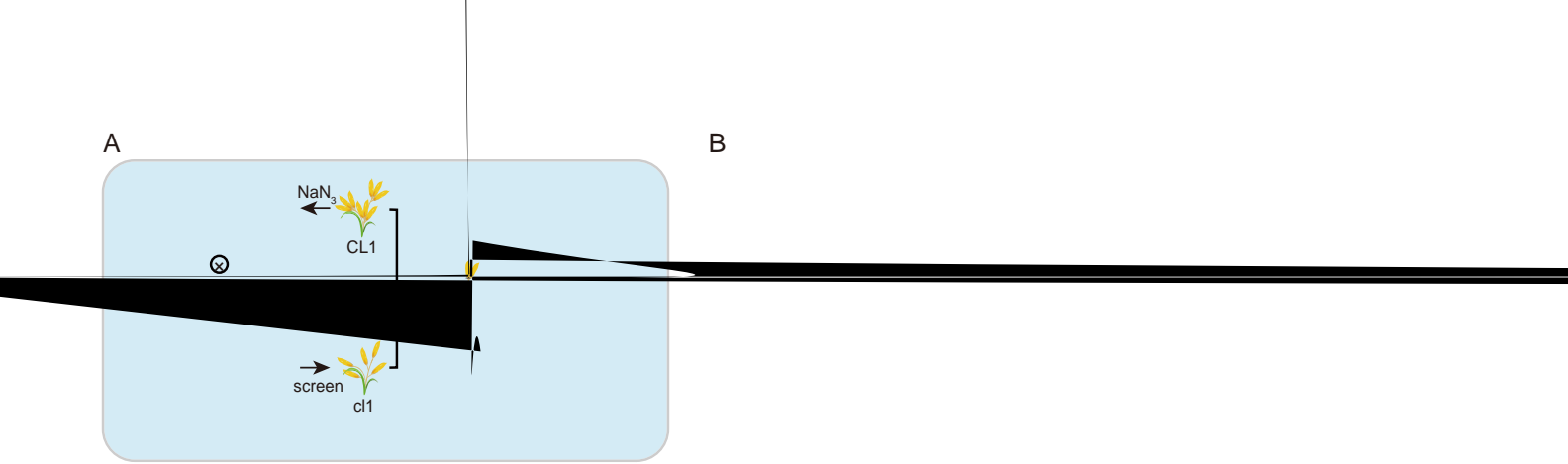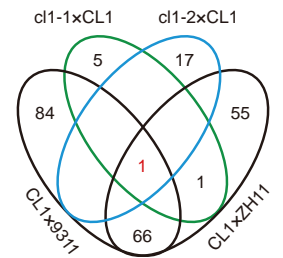
L

M

no detectable differences in grain size and plant height among CL1, *cl1-1*, *cl1-2*, and NCL1 (Fig. 3, C to E, and fig. S17). Because CL is closely associated with shortened pedicels, we first compared the expression pattern of *BRD3* in pedicels and spikelets of NCL1 and CL1. Notably, *BRD3* was up-regulated in pedicels, but not spikelets, of CL1 (Fig. 3F). To confirm this result, we also measured BR content in these tissues of both lines. Consistent with the expression pattern of *BRD3*, the castasterone level was only ~20% lower in CL1 spikelets, yet ~70% lower in CL1 pedicels, compared to NCL1 spikelets and pedicels (Fig. 3G).

We further conducted RNA in situ hybridization to determine the spatiotemporal expression pattern of *BRD3* during panicle development. During the development of NCL1 inflorescences, *BRD3* expression was very weak and not specific to any tissues (Fig. 3, H and I). By contrast, we detected specific signal with

A

Relative expression

0.25
0.20
0.15
0.10
0.05
0.00

ZH11 NCL1 CL1 CL2 CL3 CL4

***
***
***
***

B

Castasterone (ng g⁻¹)

1.2

0.8

0.4

0

NCL1   CL1

***

C

NCL1

CL1

cl1-1

cl1-2

D

E

F

0.3

0.2

0.1

0

Spikelet   Pedicel

G

H

PBM   PBM   PBM
        PBM
     PBM   PBM
PBM   PBM

NCL1   CL1

I

SBM   SBM   SBM
SBM   SBM   SBM   SBM
        SBM   SBM
SBM   SBM   SBM   SBM
                        SBM

NCL1   CL1   CL1

J

FM
        FM
      Ped
Ped

NCL1   CL1

K

SM   SM

              Ped
Ped

NCL1   CL1

L

FM   FM
     SM
FM
Ped   Ped   Ped

Ped
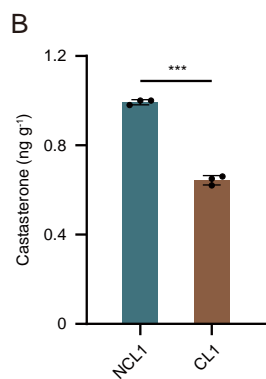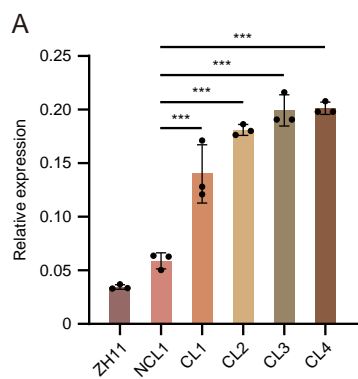
NCL1   CL1
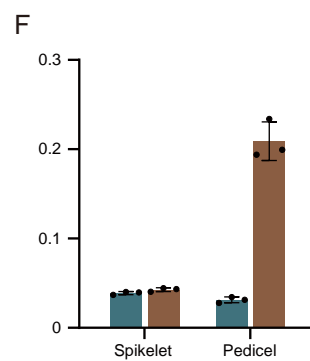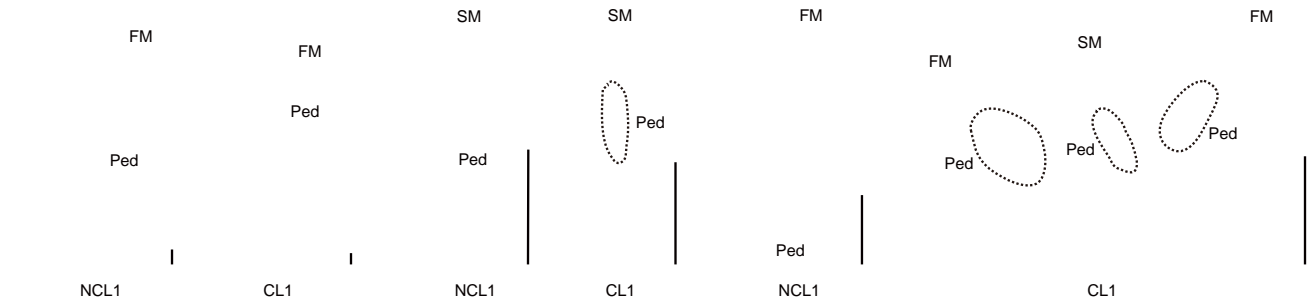
top-down development in SBM, but not PBM, of CL1 panicles (Fig. 3, H and I). At the stage of SM or FM development, *BRD3* expression was specifically detected at the base of spikelets, corresponding to the pedicel positions, in CL1 but not NCL1 (Fig. 3, J to L). As a negative control, no signal was detected when *BRD3* was used as the sense probe (fig. S18). The strong relationship between *BRD3* expression pattern and plant phenotype suggests that spatial enhancement of *BRD3* expression gives rise to the enhanced grain number, with no impact on grain size.

Spatial expression of GSK2 produces CL

Because spatial up-regulation of BRD3 in CL1 suppresses BR biosynthesis and BRs function through the BR signaling pathway, spatial suppression of BR signaling could also enable CL development. GSK2 is a central negative regulator of BR signaling (7), and we have generated many transgenic plants overexpressing the activated form of GSK2 (aGSK2) with or without the fusion of different tags, including FLAG, green fluorescent protein (GFP), and GFP-Myc (7, 32). Whereas most of these plants (*GFP-aGSK2*, *GFP-Myc-aGSK2*, *aGSK2*) showed typical BR-defective phenotypes such as dwarfism and small grains, the *FLAG-aGSK2* overexpression line exhibited dense and compact panicles due to the clustered growth of multiple spikelets (between two and six, three in most cases; Fig. 4, A and B). Immunoblotting analyses confirmed that the phenotype severity coincided with FLAG-aGSK2 protein levels (Fig. 4, C and D). Notably, in all the three lines analyzed, grain number increased from 20 to 31.2% compared to ZH11 (fig. S19). Upon further analysis, one *FLAG-aGSK2* line possessed 62% more secondary branches as well as more spikelets on the secondary branches, with no differences in primary branch numbers, compared to ZH11 (fig. S19). Clearly, many of these characteristics bear a strong resemblance to CL phenotypes.

The BR-related analyses, including lamina inclination assays (fig. S20), evaluation of BR biosynthesis genes (fig. S21), and BR quantifications (fig. S22), all suggested that the FLAG-aGSK2 protein is functional, but its ability to suppress BR signaling is likely weakened. Notably, no difference was detected in term of the grain size and grain weight, and only a slight reduction of plant height was observed in *FLAG-aGSK2* compared to ZH11 (Fig. 4E and fig. S23). The specific enhancement of grain number in *FLAG-aGSK2* resulted in a 14.7 to 27% increase in grain yield per plant compared to ZH11 (fig. S19). We then evaluated GSK2 protein levels in pedicels and spikelets of *FLAG-aGSK2*. In the two independent lines tested, FLAG-aGSK2 accumulated to high levels in pedicels but much less in spikelets (Fig. 4F). By contrast, GFP-aGSK2 was abundant in

spikelets but was barely detected in pedicels (Fig. 4G).

We further performed immunofluorescence analysis to compare the spatial distribution of the two fusion proteins in their corresponding plants during panicle development. Notably, whereas both FLAG-aGSK2 and GFP-aGSK2 were not detected at the PBM (Fig. 4H), a strong fluorescent signal was detected at the SBM of only *FLAG-aGSK2*, but not *GFP-aGSK2* (Fig. 4I). The diffused expression of FLAG-aGSK2 in the whole inflorescence is consistent with the overall compact morphology of the panicles (Fig. 4I). With further development, both the proteins were abundantly expressed in the SM as well as the FM, whereas only FLAG-aGSK2, but not GFP-aGSK2, was evidently expressed in pedicels (Fig. 4, J and K). These analyses suggest that the FLAG tag somehow affected the distribution of the fusion protein. Like the case of *BRD3* in NCL1 and CL1, these molecular characterizations were consistent with the plant phenotypes, demonstrating that the CL phenotype is regulated by spatially restricted BR function conferred by specific expression of *BRD3* or FLAG-aGSK2.

Manipulation of BRs modulates CL severity

To assess the impact of BRs on the CL phenotype, we crossed CL1 with two BR-enhanced plants, including *m107*, a mutant carrying overexpressed BR biosynthesis gene *DWARF11* (*D11*) (33), and *Gi-2*, an RNA interference (RNAi) line targeting GSK3-like family genes (7). Introducing either *m107* or *Gi-2* into CL1 resulted in the elimination of the CL phenotype (fig. S24). In addition, treating CL1 with BL mitigated the CL severity (fig. S25). Moreover, we directly edited *D11* in CL1 using CRISPR-Cas9 and found that knockout of *D11* (CL1 *d11-cc*) substantially intensified the CL phenotype (fig. S26). Notably, a mild *d11* allele displayed a WCL phenotype, and the double mutant *FLAG-aGSK2 d11* exhibited clustered growth of almost all spikelets (fig. S27). Both *FLAG-aGSK2 d11* and CL1 *d11-cc* had short, dense, and erect panicles, yet showing greatly reduced grain size (figs. S26 and S27).

Furthermore, we introduced *FLAG-aGSK2* into CL1 through transformation. Notably, CL1 *FLAG-aGSK2* exhibited markedly heightened CL severity compared to CL1, with clustered growth of up to eight spikelets (Fig. 4, L and M, and fig. S28). These results demonstrated that defective BR signaling amplifies the CL phenotype induced by BR deficiency.

GSK2 phosphorylates OsMADS1 to promote its stability

GSK2 acts as a regulator of various BR responses by targeting multiple downstream components. To delve deeper into the mechanism of BR regulation in CL, we carried out yeast two-hybrid screens using GSK2 as the

bait, resulting in the identification of OsMADS1, a potential CL regulator (34), as a candidate interacting protein of GSK2. The interaction in yeast was first confirmed using the full-length coding sequence of *OsMADS1* (Fig. 5A). OsMADS1 contains four domains, including the MADS domain (M), the intervening domain (I), the keratin-like domain (K), and the C-terminal domain (C). We generated domain-based deletions and found, only with the presence of M, I, and K domains, that OsMADS1 can interact with GSK2 (Fig. 5B). The interaction was further confirmed in *Nicotiana benthamiana* cells using split-luciferase complementation analysis (fig. S29) and was also verified by pull-down assay, showing that GSK2 fused with glutathione S-transferase (GST-GSK2) was able to interact with OsMADS1 fused with maltose binding protein (MBP-OsMADS1), as well as with MBP-tagged BRASSINAZOLE RESISTANT 1 (MBP-OsBZR1), the well-known GSK2 substrate, as a positive control (Fig. 5C). Together, these analyses demonstrated that GSK2 interacts with OsMADS1.

Previous work has shown that GSK2 kinase could phosphorylate its substrates (7). To test whether GSK2 phosphorylates OsMADS1, we conducted in vitro phosphorylation assay using the recombinant proteins GST-GSK2 and MBP-OsMADS1. With the addition of adenosine 5′-triphosphate (ATP), we detected a clear band shift corresponding to the high–molecular-weight bands of OsMADS1, and calf intestinal alkaline phosphatase (CIP) treatment eliminated these bands (fig. S29), demonstrating that GSK2 phosphorylation causes the OsMADS1 mobility shift.

Mass spectrometry analysis of the phosphorylated OsMADS1 identified three phosphorylation sites, located at position 16 for serine (S16), 20 for threonine (T20), and S138 (Fig. 5D and fig. S30). To analyze the effect of these three loci on OsMADS1, we created its phosphor-dead form by mutating all three loci to alanine (OsMADS1^{TA}), which cannot be phosphorylated by GSK2 in vitro (fig. S29), and its phosphor-mimic form by mutating to aspartate (OsMADS1^{TD}). Mutations of the single site at S138 were also performed, resulting in OsMADS1^{S138A} and OsMADS1^{S138D}, respectively. When each of these different forms of OsMADS1 was fused with a GFP tag and introduced into *N. benthamiana*, we found that the fluorescence intensity representing the OsMADS1^{TD} protein level was extraordinarily strong (Fig. 5E). We further detected the expression levels of the different proteins using immunoblotting and obtained the same result, namely, that OsMADS1^{TD} accumulated markedly relative to the wild-type OsMADS1 (Fig. 5F). In addition, both OsMADS1^{TA} and OsMADS1^{S138A} were reduced, whereas OsMADS1^{S138D} tended to be enhanced (Fig. 5F). Moreover, BL treatment markedly induced the instability of the
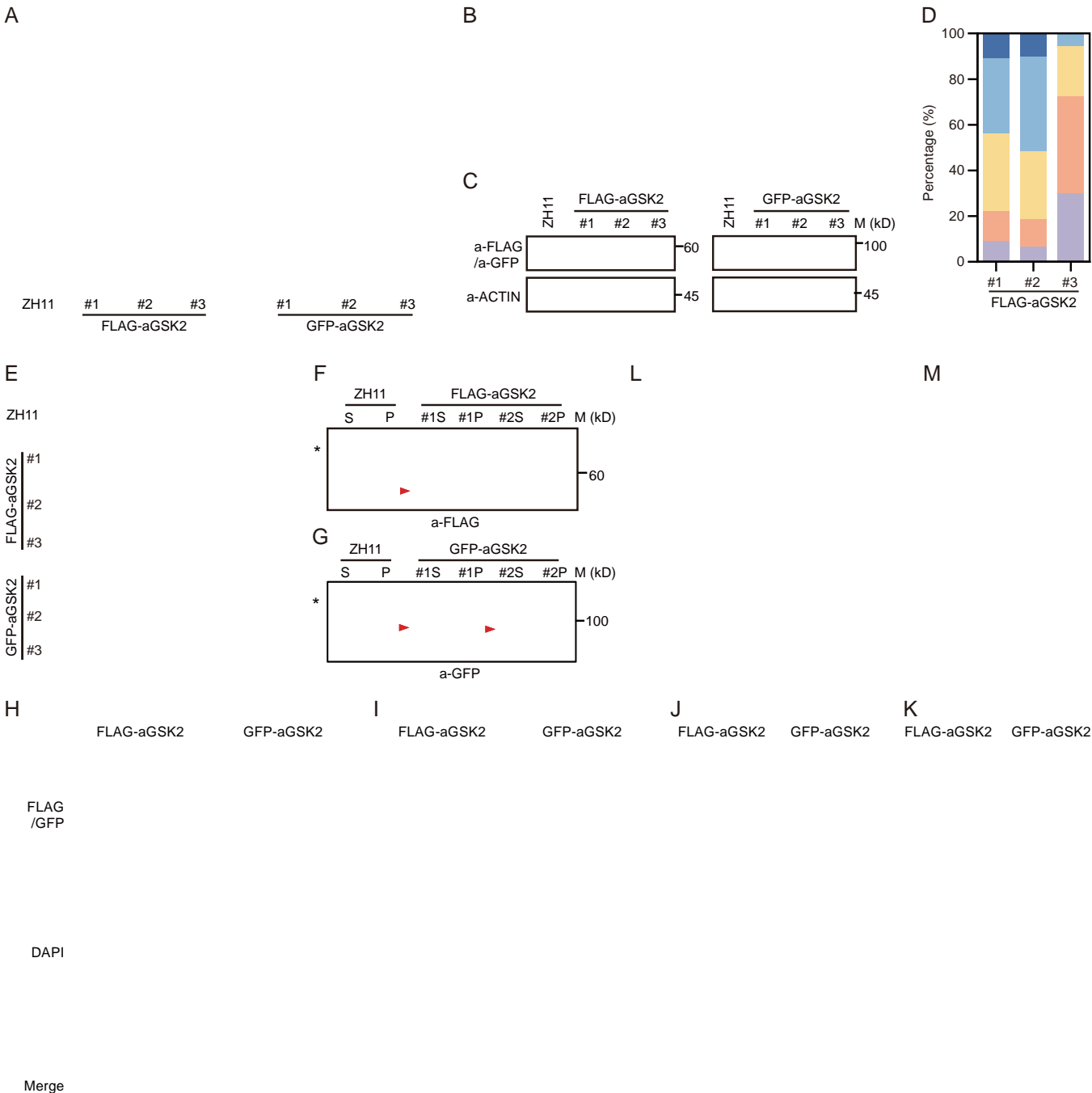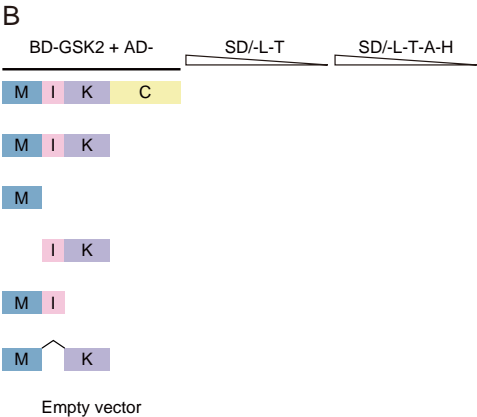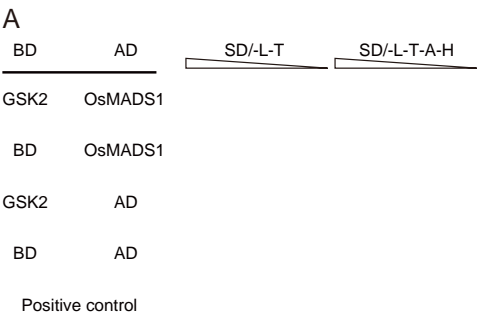
Fig. 4. Spatially specific expression of GSK2 produces CL. (A) Panicles of ZH11 and the transgenic plants. Scale bars: 2 cm. **(B)** Different cluster types in *FLAG-aGSK2* plants. Scale bar: 1 cm. **(C)** Detection of the fusion proteins in the transgenic plants by immunoblotting analyses. ACTIN was detected as control. M (kD), marker size indicated in kilodaltons. **(D)** Percentages of grain numbers belonging to different cluster types in the three *FLAG-aGSK2* lines, with 15 panicles analyzed for each line. **(E)** Comparison of grain size in different GSK2-related plants. Scale bar: 5 mm. **(F and G)** Detection of the fusion proteins in spikelets (S) and pedicels (P) of the plants by immunoblotting. Asterisk (*) represents a nonspecific band indicating equal protein loading. Arrowheads indicate target protein signals. **(H to K)** Immunofluorescence analysis of the fusion proteins during inflorescence development in *FLAG-aGSK2* and *GFP-aGSK2*, pedicel. The expression in the presumed pedicel positions were circled. Scale bars: 100 mm. **(L and M)** Comparison of the panicles and primary branches of CL1, *FLAG-aGSK2* and the double mutant. Scale bars: 2 cm (L) and 1 cm (M).

OsMADS1-FLAG fusion protein (fig. S29). These results strongly suggested that phosphorylation of OsMADS1 by GSK2 enhances the stability of the OsMADS1 protein.

OsMADS1 accumulates in pedicels of CLs

Given that GSK2 targets and promotes OsMADS1, the OsMADS1 protein should also specifically accumulate in CL plants in the same way that

FLAG-aGSK2 protein or BRD3 transcripts do. To test this notion, we analyzed OsMADS1 protein levels in spikelets and pedicels of *FLAG-aGSK2* and *GFP-aGSK2* lines. Compared to wild

A

BD	AD	SD/-L-T	SD/-L-T-A-H
GSK2	OsMADS1		
BD	OsMADS1		
GSK2	AD		
BD	AD		

Positive control

B

BD-GSK2 + AD-   SD/-L-T   SD/-L-T-A-H

| M | I | K | C |
| M | I | K |
| M |
I	K
M	I
M	K

Empty vector

ZH11   #1S   #2S

Spikelet

C

MBP-OsMADS1	+	+	-	-
GST-GSK2	-	+	-	+
MBP-OsBZR1	-	-	+	+
GST	+	-	+	-	M (kD)

pull-down
a-MBP   75

input
a-MBP   75

input   75
a-GST   35

D

S16 T20   S138

| M | I | K | C |

E

F

OsMADS1-GFP   OsMADS1^TA-GFP   OsMADS1^TD-GFP   OsMADS1^S138A-GFP   OsMADS1^S138D-GFP

M (kD)

a-GFP   75

a-HSP   75

a-NPT   25
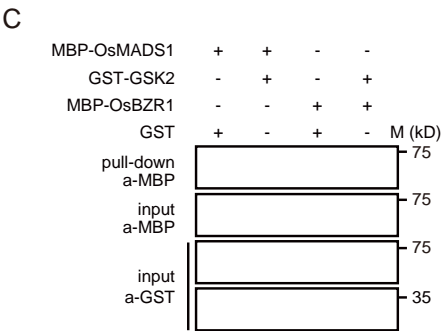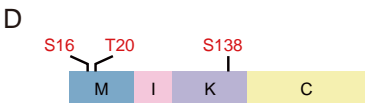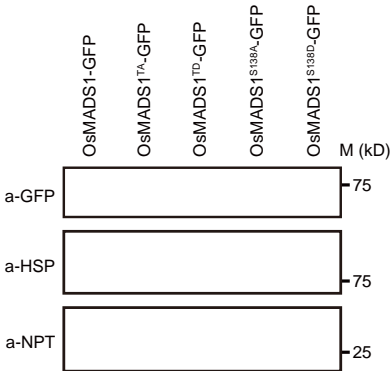
K

ZH11   OsMADS1-OE   GFP-aGSK2

L

M

N

type, in spikelets, OsMADS1 was more abundant in *GFP-aGSK2*, but of similar abundance in *FLAG-aGSK2* (Fig. 5G). By contrast, in pedicels, OsMADS1 strongly accumulated in *FLAG-aGSK2*, but not in *GFP-aGSK2* (Fig. 5H). These data clearly demonstrated that the distribution patterns of OsMADS1 and GSK2 are highly similar in either *GFP-aGSK2* or *FLAG-aGSK2* (Figs. 4, F and G, and 5, G and H). In addition, the distribution patterns are also consistent with the plant phenotypes: *GFP-aGSK2* has smaller grains, whereas *FLAG-aGSK2* has shortened pedicels and normal grain size (Fig. 4E).

We then extended the analysis to CL1 and NCL1. Consistently, OsMADS1 levels were higher in pedicels, but not spikelets, of CL1 compared to NCL1 (Fig. 5, I and J). These patterns were similar to those observed in *FLAG-aGSK2*. Taken together, these results demonstrated that OsMADS1 acts downstream of GSK2 to mediate BR regulation of CL development.

Knockdown of *OsMADS1* abolishes CL phenotype

Similar to GSK2, OsMADS1 has been characterized as a negative regulator of grain size (*35*, *36*). Furthermore, OsMADS1 has been implicated in regulating meristem identity and potentially enhancing spikelet number (*37–39*). Examination of *OsMADS1*-overexpressing plants (*OsMADS1-OE*) confirmed that its grains were notably smaller, like *GFP-aGSK2*, than the wild type ZH11 (Fig. 5K). Notably, the clustered growth of two or three spikelets was clearly observed on almost every panicle, and some branches showed strong resemblance of typical CL characteristics (Fig. 5L). The occurrence of CL phenotype in *OsMADS1-OE* indicated that OsMADS1 mediates GSK2-regulation of the CL trait.

To test that notion, we performed RNAi on *OsMADS1* in CL1 (*OsMADS1-RNAi*). Among the lines generated with suppressed expression of *OsMADS1* (Fig. 5M), the CL phenotype was eliminated (Fig. 5N), indicating that OsMADS1 is necessary for the CL phenotype. These findings, coupled with the analyses, collectively established that OsMADS1 functions downstream of GSK2 to mediate CL development.

Specific accumulation of *OsMADS1* in CL1's SBMs

To provide direct evidence for the spatial distribution pattern of OsMADS1 protein, we performed immunofluorescence analysis to track the protein abundance during panicle development. Although we could not detect OsMADS1 proteins at the PBM of both CL1 and NCL1, the specific fluorescent signal was detected at the SBM of only CL1, but not NCL1 (Fig. 6, A and B). In addition, the signal was restricted to the apically located SBM, which might be in the transition stage to SM, implying the involvement of OsMADS1 in this process. With further development, OsMADS1 started to be abundantly expressed in the SM as well as the FM in both NCL1 and CL1 (Fig. 6, C and D), consistent with the core function of OsMADS1 as a flower organ regulator reported previously (*37*, *40–42*). Notably, a distinct OsMADS1 fluorescent signal was also detected in the center of pedicels of CL1, where the signal was absent in NCL1. This specific expression pattern was fully consistent with the above immunoblotting results and reminiscent of the RNA in situ expression of *BRD3*: Compared to NCL1, both *BRD3* transcripts and OsMADS1 proteins accumulated specifically in the SBM as well as in pedicel-corresponding cells of CL1. Taken together, these results demonstrated that the specific accumulation of OsMADS1 mediates the occurrence of CL caused by the specific distribution of either *BRD3* or GSK2.

OsMADS1 targets a *TERMINAL FLOWER1*-like gene

To gain deeper insights into the function of OsMADS1, a transcription factor, we conducted a combined analysis of chromatin immunoprecipitation sequencing (ChIP-seq) and RNA sequencing (RNA-seq), aiming to identify the target genes regulated by OsMADS1. Using young panicles of *OsMADS1-OE* plants (~5 mm in length) as materials, the ChIP-seq analysis detected a total of 1650 OsMADS1-bound peaks associated with 1320 genes (Fig. 6E). Simultaneously, the RNA-seq analysis identified 1354 differentially expressed genes (DEGs) (Fig. 6E). By performing an overlapping analysis of the two datasets, we identified 46 genes as both OsMADS1-bound genes and DEGs regulated by OsMADS1 (Fig. 6E and table S2), which were thus considered as the direct targets of OsMADS1. According to the rice database (https://ricedata.cn/), 15 of them have been functionally characterized (Fig. 6F). Among them, *RICE CENTRORADIALIS2* (*RCN2*) stood out as the most promising target regulating CL development, which ranked third in terms of enrichment fold (~9.84-fold) in the ChIP-seq, and second in terms of expression change (~5.83-fold) in the RNA-seq (Fig. 6F). In addition, further inspection using the Integrated Genome Viewer (*43*) indicated that the binding peak on *RCN2* is highly specific (Fig. 6G). Notably, previous studies have shown that all four *RCN* genes in rice, *RCN1* to *RCN4*, serving as the rice counterparts of *Arabidopsis TERMINAL FLOWER 1* (*TFL1*), play crucial roles in promot-

number with 81.5 and 39.7% more grains per panicle compared to R498 and CL1, respectively (Fig. 7, E and F). In addition, CL5 possessed other advantageous traits such as a thick culm, heavier grains (fig. S35), and high yield (Fig. 7G), illustrating the promising potential of combining *CL* and *Gn1a* for enhancing rice yield.

BR alteration in clustered growth in other species

Although we demonstrated that BR depletion controls CL in rice (Fig. 7H), we wanted to know whether this represent a general mechanism underlying clustered growth across plant species. Cluster peppers (*Capsicum annuum* L. var. *fasciculatum*) display multiple flowers clustered on a single flower bud formation node, whereas common peppers (*Capsicum annuum* L.) have only one flower attached to the node. We measured the BR content in pedicels of Tianyu 2 (TY2), a common pepper, and TY2^{CL}, a cluster pepper showing clustered flowers and shortened pedicels while closely resembling TY2 in vegetative and reproductive morphology (Fig. 7, I and J). Like CL1 and NCL1, the castasterone level was lower in TY2^{CL} pedicels compared to TY2 (Fig. 7K). Conversely, the 6-deoxocastasterone level, the precursor of castasterone, was higher in TY2^{CL} pedicels (Fig. 7K), indicating a possible loss of function in the BR synthase responsible for converting 6-deoxocastasterone to castasterone.

We also measured the BR content in the pedicels of the vine *Rosa chinensis* (*Rosa* "Parkdirektor Riggers") and the vine *Rosa* sp. (*Rosa* "Angela"), which displays the clustered flowers and shortened pedicels (Fig. 7, L and M). Like TY2 and TY2^{CL}, the castasterone level in *Rosa* "Angela" pedicels was lower compared to *Rosa* "Parkdirektor Riggers," whereas the 6-deoxocastasterone level exhibited the opposite trend (Fig. 7N). These consistent findings indicate that BR distribution may play a general role in regulating the clustered growth and inflorescence structure.

Discussion

We unraveled the genetic basis underlying the historic CL germplasm, shedding light on the development of CL and its association with enhanced grain number, a crucial determinant of yield. We demonstrated that defective BR catabolism or signaling contributes to spikelet clustering and increased grain number, mediated by the specific spatial expression of *BRD3* transcripts, GSK2 protein, OsMADS1 protein, and *RCN2* transcripts. During CL's panicle development, the activation of *BRD3* in SBM triggers BR degradation, which enhances GSK2 stability, promotes OsMADS1 accumulation, and subsequently increases *RCN2* expression. As a result, the identity of SM is suppressed, leading to a delayed transition from BM to SM, ultimately yielding more SBMs and additional SMs formed adjacent to the ter-

minal spikelet (Fig. 7H). Overall, our study exemplifies the successful utilization of natural rice germplasm resources harboring beneficial alleles to breed superior rice strains, from gene cloning to the dissection of the underlying molecular mechanisms.

KNOX transcription factors play a crucial role in the establishment and maintenance of the shoot apical meristem (SAM) (*48*). In *Arabidopsis*, BREVIPEDICELLUS (BP), a KNOX transcription factor, has been shown to regulate pedicel development (*48*). In rice, ORYZA SATIVA HOMEBOX1 (OSH1), the closest ortholog of BP, targets and activates BR catabolic genes, including *BRD3*, to maintain SAM activity (*49*). Therefore, the degradation of BRs should also promote the activity of SBM and SM. In our study, we observed an increase in grain number accompanied by shortened pedicels, and the expression of *BRD3* was detected sequentially in both the meristem cells and pedicel cells, suggesting a potential derivation of pedicels from meristem cells. Our findings imply that large structural variations preceding the *BRD3* gene may be responsible for the spatially specific increase in *BRD3* expression observed in CL. Although the detailed mechanism requires further exploration, one possibility is that these structural variations enhance chromatin accessibility, allowing the entry of transcription factors, such as OSH1, to promote *BRD3* expression.

Constitutive activation of *BRD3* in a transferred DNA (T-DNA) insertion mutant results in severe developmental defects, whereas moderately increased expression of *BRD3* in the heterozygote leads to higher grain number but smaller grains (*29*). Therefore, the practical application of *CL* in crop improvement can be attributed to two main factors related to *BRD3* expression: spatially specific expression and optimal expression. The resulting spatial distribution of BRs provides beneficial effects while preventing the reduction in grain size typically observed in BR-defective mutants, showcasing its practical applicability in crop improvement. Together with our previous research on the distribution of cytokinins and auxins (*50*, *51*), this work highlights the potential of optimizing hormone distributions to achieve desirable traits while mitigating negative associations in crop improvement efforts. Improving grain yield is intricately linked to expanding source supply, influenced by various factors such as source capacity, growth conditions (light, water, temperature, nutrients), and fertilizers. Although introduction of CL into several different modern cultivars all resulted in yield improvement, we observed distinct effects in different locations and genetic backgrounds. Considering that CL is influenced by BR content and each rice may exhibit variable BR levels, it is crucial to extensively test the effectiveness of CL in diverse contexts.

Materials and methods summary

Plant growth, suppressor screening, and segregating populations

For field plot analysis, each material was planted with a row interspace of 20 cm and plant interspace of 17.1 cm, with ~33 plants per square meter. At least four plots were planted as biological replicates. The border plants were removed from each plot to avoid margin effects during measurements. For experiments requiring seedling analysis, plants were grown in a growth chamber at 30°C with 10 hours light for day and 28°C with 14 hours dark for night. Half-strength Murashige and Skoog (½-MS) solution was provided as the nutrient source. For suppressor screening, dry CL1 seeds were incubated in sodium azide (1 mM in phosphate buffer pH 3.0) for 6 hours. After a thorough wash with tap water, the seeds were germinated and planted. A total of 10,000 individual lines were harvested, and 16 plants of each line were grown for mutant screening. Four segregating populations were generated by crossing CL1 with ZH11, 9311, *cl1-1*, and *cl1-2*, respectively. For each population, pooled DNAs from NCL plants and CL plants were prepared for BSA. Numbers of individual plants used for DNA pools from each population were as follows: 36 NCL and 34 CL from CL1 × ZH11, 24 NCL and 31 CL from CL1 × 9311, 31 NCL and 33 CL from CL1 × *cl1-1*, and 20 NCL and 19 CL from CL1 × *cl1-2*.

RNA in situ hybridization

Specific fragments of *BRD3* and *RCN2* were amplified by PCR with primers listed in table S1. The fragments were subsequently inserted into the pEASY-Blunt Simple Cloning Vector (TransGen) for in vitro RNA transcription. Sense and antisense RNA probes were produced using T7 transcriptase and labeled with digoxigenin (Roche). Young panicle tissues from NCL1 and CL1 were collected and fixed in FAA (45% ethanol, 6% glacial acetic acid, and 5% formaldehyde) at 4°C overnight in a vacuum, dehydrated, and embedded in Paraplast Plus (Sigma-Aldrich, St. Louis). Tissue sections were prepared using a microtome (RM2235; Leica, Wetzlar) and then affixed to Poly-Prep slides (Sigma-Aldrich, St. Louis).

In vitro phosphorylation and mass spectrum analysis

One microgram of GST-GSK2 and 2 mg of MBP-OsMADS1 or MBP-OsMADS1^{TA} were incubated in the kinase buffer [10 mM Tris-HCl (pH 7.4), 50 mM NaCl, 6 mM MgCl$_2$, 0.5 mM dithiothreitol] with or without ATP and CIP (NEB) at 30°C for 2 hours. Phos-tag^{TM} SDS–polyacrylamide gel electrophoresis (PAGE) was used to separate the phosphorylation protein following the instruction of the product Phos-tag^{TM} Acrylamide (Wako). To identify the phosphorylation sites, 4 mg of recombinant

MBP-OsMADS1 or MBP-OsMADS1^{TA} proteins were phosphorylated by 2 mg of GST-GSK2 for 1 hour in vitro. Phos-tag^{TM} SDS-PAGE was used to separate the phosphorylation protein. The target protein bands were cut after one-step blue staining (Biotium). The LC-MS/MS detection and analysis were conducted by the Shanghai Luming Biological Technology Co., Ltd. (Shanghai, China).

Immunofluorescence detection

An 8-mm-thick section was cut from paraffin-embedded young panicle tissues for detection. The slides were deparaffinized, rehydrated, and subjected to epitope retrieval by boiling in 1× All-purpose Powerful Antigen Retrieval Solution (Beyotime) for 20 min at 95°C, and set to cool for 30 to 40 min. The slides were washed two times in 1× Immunol Staining Wash Buffer (Beyotime) for 10 min each, blocked in Immunol Staining Blocking Buffer (Beyotime) for 60 min at room temperature, and then rinsed two times in 1× Immunol Staining Wash Buffer (Beyotime) for 10 min each. The primary antibody for OsMADS1 (1:50; Abclonal, Cat#A20328), or for FLAG-aGSK2 (anti-FLAG, 1:50; Sigma, Cat#F1804), or for GFP-aGSK2 (anti-GFP, 1:50; Abmart, Cat#M20041), was used for incubation overnight at 4°C. The specimen was rinsed three times in 1× Immunol Staining Wash Buffer (Beyotime) for 5 min each, and then incubated in the Goat anti-Rabbit IgG (H+L) Highly Cross-Adsorbed Secondary Antibody, Alexa Fluor^{TM} Plus 555 (1:400; Invitrogen, Cat#A32732) or Goat anti-Mouse IgG (H+L) Highly Cross-Adsorbed Secondary Antibody, Alexa Fluor Plus 488 (1:400; Invitrogen, Cat#A32723) at room temperature for 60 min in dark. The slides were further rinsed three times in 1× Immunol Staining Wash Buffer (Beyotime) for 5 min each, and then covered using coverslips filled with Antifade Mounting Medium with 4',6-diamidino-2-phenylindole (DAPI; Beyotime). Fluorescence was captured with a confocal laser scanning microscope (LSM 980; Zeiss, Oberkochen).

ChIP-seq and RNA-seq

About 1 g of young panicles at the 5-mm stage of *OsMADS1-OE* were used for ChIP-seq. Tissue fixation, nuclei extraction, and chromatin immunoprecipitation were performed using anti-OsMADS1 (1:100; Abclonal, Cat#A20328) antibody. The ChIP-seq DNA libraries were sequenced using the Illumina HiSeqTM2000 platform. After quality control, BWA software was used to align the clean reads against the Nipponbare reference genome (IRGSP1.0). MACS software was used for peak calling on a genome-wide basis, and the threshold for screening significant peak was q-value < 0.05. Significant peaks were assigned to the nearest gene. For RNA-seq, about 1 g of young panicles

at the 5-mm stage of *OsMADS1-OE* and ZH11 were collected, and total RNA was extracted from each of three biological replicates using TRIzol reagent (Invitrogen). Sequencing libraries were generated using NEBNext Ultra RNA Library Prep Kit for Illumina (NEB), following the manufacturer's recommendations, and sequenced on Illumina NovaSeq platform. After cleaning up raw sequence reads, the clean reads were mapped to the Nipponbare reference genome (IRGSP1.0). The differentially expressed genes were analyzed using the edgeR package. Genes with a false discovery rate (FDR) < 0.05 and log$_2$(fold change) > 1 were assigned as differentially expressed.

REFERENCES AND NOTES

1. T. Sasaki, B. Burr, International Rice Genome Sequencing Project: The effort to completely sequence the rice genome. *Curr. Opin. Plant Biol.* **3**, 138–142 (2000). doi: 10.1016/S1369-5266(99)00047-3; pmid: 10712951

2. X. Huang *et al.*, Natural variation at the *DEP1* locus enhances grain yield in rice. *Nat. Genet.* **41**, 494–497 (2009). doi: 10.1038/ng.352; pmid: 19305410

3. M. Ashikari *et al.*, Cytokinin oxidase regulates rice grain production. *Science* **309**, 741–745 (2005). doi: 10.1126/science.1113373; pmid: 15976269

4. E. J. Kim, E. Russinova, Brassinosteroid signalling. *Curr. Biol.* **30**, R294–R298 (2020). doi: 10.1016/j.cub.2020.02.011; pmid: 32259497

5. H. Tong, C. Chu, Functional specificities of brassinosteroid and potential utilization for crop improvement. *Trends Plant Sci.* **23**, 1016–1028 (2018). doi: 10.1016/j.tplants.2018.08.007; pmid: 30220494

6. T. M. Nolan, N. Vukašinović, D. Liu, E. Russinova, Y. Yin, Brassinosteroids: Multidimensional regulators of plant growth, development, and stress responses. *Plant Cell* **32**, 295–318 (2020). doi: 10.1105/tpc.19.00335; pmid: 31776234

7. H. Tong *et al.*, DWARF AND LOW-TILLERING acts as a direct downstream target of a GSK3/SHAGGY-like kinase to mediate brassinosteroid responses in rice. *Plant Cell* **24**, 2562–2577 (2012). doi: 10.1105/tpc.112.097394; pmid: 22685166

8. J. Li, K. H. Nam, Regulation of brassinosteroid signaling by a GSK3/SHAGGY-like kinase. *Science* **295**, 1299–1301 (2002). doi: 10.1126/science.1065769; pmid: 11847343

9. J. H. Youn, T. W. Kim, Functional insights of plant GSK3-like kinases: Multi-taskers in diverse cellular signal transduction pathways. *Mol. Plant* **8**, 552–565 (2015). doi: 10.1016/j.molp.2014.12.006; pmid: 25655825

10. Z. Hong *et al.*, A rice brassinosteroid-deficient mutant, *ebisu dwarf (d2)*, is caused by a loss of function of a new member of cytochrome P450. *Plant Cell* **15**, 2900–2910 (2003). doi: 10.1105/tpc.014712; pmid: 14615594

11. S. Tanabe *et al.*, A novel cytochrome P450 is implicated in brassinosteroid biosynthesis via the characterization of a rice dwarf mutant, *dwarf11*, with reduced seed length. *Plant Cell* **17**, 776–790 (2005). doi: 10.1105/tpc.104.024950; pmid: 15705958

12. C. Yamamuro *et al.*, Loss of function of a rice brassinosteroid insensitive1 homolog prevents internode elongation and bending of the lamina joint. *Plant Cell* **12**, 1591–1606 (2000). doi: 10.1105/tpc.12.9.1591; pmid: 11006334

13. L. Song *et al.*, Reducing brassinosteroid signalling enhances grain yield in semi-dwarf wheat. *Nature* **617**, 118–124 (2023). doi: 10.1038/s41586-023-06023-6; pmid: 37100915

14. J. Tian *et al.*, Teosinte ligule allele narrows plant architecture and enhances high-density maize yields. *Science* **365**, 658–664 (2019). doi: 10.1126/science.aax5482; pmid: 31416957

15. T. Sakamoto *et al.*, Erect leaves caused by brassinosteroid deficiency increase biomass production and grain yield in rice. *Nat. Biotechnol.* **24**, 105–109 (2006). doi: 10.1038/nbt1173; pmid: 16369540

16. K. Ramiah, S. Jobitharaj, S. D. Mudaliar, Inheritance of characters in rice, Part IV. *Mem. Dept. Agric. India Bot. Ser.* **18**, 229–259 (1931).

17. N. E. Jodon, Inheritance and linkage relationships of a chlorophyll mutation in rice. *Agron. J.* **32**, 342–346 (1940). doi: 10.2134/agronj1940.00021962003200050004x

18. N. E. Jodon, Inheritance of some of the more striking characters in rice. *J. Hered.* **48**, 181–192 (1957). doi: 10.1093/oxfordjournals.jhered.a106718

19. S. Nagao, M. E. Takahashi, Genetical studies on rice plant, XXVII. Trial construction of twelve linkage groups in Japanese rice. *J. Fac. Agric. Hokkaido Univ.* **53**, 72–130 (1963).

20. H. Chen, G. Liu, X. Zhu, S. Min, Observation and genetically analysis on character of clustered spikelets in rice. *J. Nanjing Agric. Univ.* **25**, 116–118 (2002).

21. C. Tian *et al.*, Genetic analysis and preliminary gene mapping of rice clustered spikelet mutant. *Mol. Plant Breed.* **8**, 29–34 (2010).

22. Y. Zhang *et al.*, Development of NILs with Cl gene of rice restorer and evaluation on the near-isogenic level. *Acta Agron. Sin.* **32**, 397–401 (2006).

23. L. Y. Zheng *et al.*, Morphology and mapping analysis of rice (*Oryza sativa* L.) clustered spikelet (Cl) mutant. *Chin. Sci. Bull.* **48**, 559–562 (2003). doi: 10.1360/03tb9119

24. Y. Zheng *et al.*, Fine mapping and candidate gene analysis of clustered spikelet gene OsCl-6 in rice (*Oryza sativa*). *J. Agric. Biotechnol.* **26**, 1116–1123 (2018).

25. M. Nakagawa, K. Shimamoto, J. Kyozuka, Overexpression of RCN1 and RCN2, rice TERMINAL FLOWER 1/CENTRORADIALIS homologs, confers delay of phase transition and altered panicle morphology in rice. *Plant J.* **29**, 743–750 (2002). doi: 10.1046/j.1365-313X.2002.01255.x; pmid: 12148532

26. P. Prusinkiewicz, Y. Erasmus, B. Lane, L. D. Harder, E. Coen, Evolution and development of inflorescence architectures. *Science* **316**, 1452–1456 (2007). doi: 10.1126/science.1140429; pmid: 17525303

27. P. McSteen, D. Laudencia-Chingcuanco, J. Colasanti, A floret by any other name: Control of meristem identity in maize. *Trends Plant Sci.* **5**, 61–66 (2000). doi: 10.1016/S1360-1385(99)01541-1; pmid: 10664615

28. W. Wang *et al.*, Genomic variation in 3,010 diverse accessions of Asian cultivated rice. *Nature* **557**, 43–49 (2018). doi: 10.1038/s41586-018-0063-9; pmid: 29695866

29. W. Qian *et al.*, Novel rice mutants overexpressing the brassinosteroid catabolic gene CYP734A4. *Plant Mol. Biol.* **93**, 197–208 (2017). doi: 10.1007/s11103-016-0558-4; pmid: 27815670

30. T. Sakamoto *et al.*, Rice CYP734As function as multisubstrate and multifunctional enzymes in brassinosteroid catabolism. *Plant J.* **67**, 1–12 (2011). doi: 10.1111/j.1365-313X.2011.04567.x; pmid: 21418356

31. H. A. Agrama *et al.*, Genetic assessment of a mini-core subset developed from the USDA rice genebank. *Crop Sci.* **49**, 1336–1346 (2009). doi: 10.2135/cropsci2008.06.0551

32. D. Liu *et al.*, Diversification of plant agronomic traits by genome editing of brassinosteroid signaling family genes in rice. *Plant Physiol.* **187**, 2563–2576 (2021). doi: 10.1093/plphys/kiab394; pmid: 34618079

33. H. Tong *et al.*, Brassinosteroid regulates cell elongation by modulating gibberellin metabolism in rice. *Plant Cell* **26**, 4376–4393 (2014). doi: 10.1105/tpc.114.132092; pmid: 25371548

34. L. Wang *et al.*, Ectopic expression of OsMADS1 caused dwarfism and spikelet alteration in rice. *Plant Growth Regul.* **81**, 433–442 (2017). doi: 10.1007/s10725-016-0220-9

35. Q. Liu *et al.*, G-protein βγ subunits determine grain size through interaction with MADS-domain transcription factors in rice. *Nat. Commun.* **9**, 852 (2018). doi: 10.1038/s41467-018-03047-9; pmid: 29487282

36. J. Yu *et al.*, Alternative splicing of OsLG3b controls grain length and yield in japonica rice. *Plant Biotechnol. J.* **16**, 1667–1678 (2018). doi: 10.1111/pbi.12903; pmid: 29479793

37. J. S. Jeon *et al.*, leafy hull sterile1 is a homeotic mutation in a rice MADS box gene affecting rice flower development. *Plant Cell* **12**, 871–884 (2000). doi: 10.1105/tpc.12.6.871; pmid: 10852934

38. K. Prasad, S. Parameswaran, U. Vijayraghavan, OsMADS1, a rice MADS-box factor, controls differentiation of specific cell types in the lemma and palea and is an early-acting regulator of inner floral organs. *Plant J.* **43**, 915–928 (2005). doi: 10.1111/j.1365-313X.2005.02504.x; pmid: 16146529

39. D. Ren, Y. Li, G. He, Q. Qian, Multifloret spikelet improves rice yield. *New Phytol.* **225**, 2301–2306 (2020). doi: 10.1111/nph.16303; pmid: 31677165

40. S. T. Malcomber, E. A. Kellogg, Heterogeneous expression patterns and separate roles of the SEPALLATA gene LEAFY HULL STERILE1 in grasses. *Plant Cell* **16**, 1692–1706 (2004). doi: 10.1105/tpc.021576; pmid: 15208396

41. K. Prasad, P. Sriram, C. S. Kumar, K. Kushalappa, U. Vijayraghavan, Ectopic expression of rice OsMADS1 reveals

a role in specifying the lemma and palea, grass floral organs analogous to sepals. *Dev. Genes Evol.* **211**, 281–290 (2001). doi: 10.1007/s004270100153; pmid: 11466523

42. I. Khanday, S. R. Yadav, U. Vijayraghavan, Rice *LHS1/OsMADS1* controls floret meristem specification by coordinated regulation of transcription factors and hormone signaling pathways. *Plant Physiol.* **161**, 1970–1983 (2013). doi: 10.1104/pp.112.212423; pmid: 23449645

43. J. T. Robinson *et al.*, Integrative genomics viewer. *Nat. Biotechnol.* **29**, 24–26 (2011). doi: 10.1038/nbt.1754; pmid: 21221095

44. W. Zhu *et al.*, Rice *SEPALLATA* genes *OsMADS5* and *OsMADS34* cooperate to limit inflorescence branching by repressing the *TERMINAL FLOWER1* gene *RCN4*. *New Phytol.* **233**, 1682–1700 (2022). doi: 10.1111/nph.17855; pmid: 34767634

45. S. Zhang *et al.*, *TFL1/CEN*-like genes control intercalary meristem activity and phase transition in rice. *Plant Sci.* **168**, 1393–1408 (2005). doi: 10.1016/j.plantsci.2004.10.022

46. X. Yang *et al.*, miR156f integrates panicle architecture through genetic modulation of branch number and pedicel length pathways. *Rice (N. Y.)* **12**, 40 (2019). doi: 10.1186/s12284-019-0299-5; pmid: 31147794

47. B. Tu *et al.*, Loss of *Gn1a/OsCKX2* confers heavy-panicle rice with excellent lodging resistance. *J. Integr. Plant Biol.* **64**, 23–38 (2022). doi: 10.1111/jipb.13185; pmid: 34783157

48. S. J. Douglas, C. D. Riggs, Pedicel development in *Arabidopsis thaliana*. Contribution of vascular positioning and the role of the *BREVIPEDICELLUS* and *ERECTA* genes. *Dev. Biol.* **284**, 451–463 (2005). doi: 10.1016/j.ydbio.2005.06.011; pmid: 16038894

49. K. Tsuda, N. Kurata, H. Ohyanagi, S. Hake, Genome-wide study of *KNOX* regulatory network reveals brassinosteroid catabolic genes important for shoot meristem function in rice. *Plant Cell* **26**, 3488–3500 (2014). doi: 10.1105/tpc.114.129122; pmid: 25194027

50. L. Liu *et al.*, Activation of *Big Grain1* significantly improves grain size by regulating auxin transport in rice. *Proc. Natl. Acad. Sci. U.S.A.* **112**, 11102–11107 (2015). doi: 10.1073/pnas.1512748112; pmid: 26283354

51. W. Yin *et al.*, ARGONAUTE2 enhances grain length and salt tolerance by activating *BIG GRAIN3* to modulate cytokinin distribution in rice. *Plant Cell* **32**, 2292–2306 (2020). doi: 10.1105/tpc.19.00542; pmid: 32409321

52. X. Zhang, Nanopore sequencing, RNA-seq and ChIP-seq data, *Zenodo* (2024); doi: 10.5281/zenodo.10574305

53. X. Zhang, BSA data, *Zenodo* (2024); doi: 10.5281/zenodo.10574366

54. X. Zhang, Resequencing data of CL1, Zenodo (2024); doi: 10.5281/zenodo.10574479

SUPPLEMENTARY MATERIALS

science.org/doi/10.1126/science.adk8838
Materials and Methods
Figs. S1 to S35
Tables S1 and S2
References (*55–73*)
MDAR Reproducibility Checklist